Attenuated-total-reflection study of pyridine overlayers on silver films

J. Giergiel, C. E. Reed, S. Ushioda, and J. C. Hemminger
School of Physical Sciences, University of California, Irvine, California 92717
(Received 5 October 1984)

We have measured optical properties of pyridine overlayers adsorbed on silver films evaporated in ultrahigh vacuum. These properties are determined from the changes in the surface-plasmon—polariton (SPP) resonance of the silver film that occurs upon adsorption of pyridine. The SPP resonance is detected by the attenuated-total-reflection (ATR) method using the Kretschmann configuration. Submonolayer quantities of pyridine overlayer shift the position of the ATR dip linearly with coverage. The magnitude of the shift is analyzed in terms of several models. With the assumption of saturation coverage of 5×10^{14} cm^{-2}, we calculate the effective polarizability of chemisorbed pyridine to be ~14.5 Å^3. We also find that the pyridine overlayer undergoes a structural transformation after completion of the first monolayer. The resulting overlayer has a rough surface, and subsequent condensation does not occur in a layer-by-layer fashion.

I. INTRODUCTION

The theoretical models proposed to explain the large surface enhancement of Raman signal (SERS) observed in certain molecule-metal systems can be divided into two major categories.[1] The so-called molecular enhancement theories rely on adsorption-induced changes in the Raman susceptibility, whereas the "electromagnetic" theories view SERS as a manifestation of strong local fields present on metal surfaces due to various electromagnetic resonances. There is some evidence that both mechanisms are involved in real experimental situations.[1] An essential feature of the molecular enhancement theories is that they predict perturbation of the electronic structure of an adsorbed molecule or creation of new excited states of a molecule-metal system. Such states at ~1.9 eV have been reported in an electron-energy loss spectroscopy (EELS) study of the pyridine—silver (111) system, and were identified as metal-molecule charge-transfer excitations.[2] The only optical work on this system was reported by Tadjeddine and Kolb.[3] They found three near-infrared-absorption bands at 780, 910, and 950 nm for Ag(111) electrodes roughened electrochemically in the presence of pyridine. In view of the molecular enhancement theories it is important to determine the optical polarizability of metal-adsorbed pyridine in the frequency range where strong SERS effect is found, i.e., 450—750 nm.[1]

In this paper we report on the optical properties in the visible range of submonolayer and monolayers of pyridine on polycrystalline Ag films as determined by changes in the surface-plasmon—polariton resonance (SPP) of the Ag film. The sensitivity of this technique is sufficient to detect submonolayer coverages.[4–6] In Sec. II we discuss the effect of a dielectric overlayer on the SPP resonance. Section III gives pertinent experimental details as well as a description of a novel expermental arrangement for attenuated-total-reflection (ATR) spectroscopy. Results for pyridine overlayers are presented and discussed in the last section.

II. THEORETICAL BACKGROUND

Two techniques have been used in SPP studies of dielectric overlayers. The propagation technique[6] requires long plasmon-polariton lifetimes and is therefore limited to the ir range. In the ATR method,[7] the resonant excitation of SPP on the metal surface leads to a significant absorption of the incident light and therefore can be easily observed as a change in the reflected light intensity. We used the Kretschmann geometry[7] in which a metal film is evaporated onto a glass prism. The purpose of the prism is to increase the wave vector of the incident light so that its component along the interface can match the $k_{||}$ vector of the SPP at the metal-dielectric interface. The reflectivity dip observed in the ATR spectra is due to the resonant excitation of SPP at the metal-dielectric interface and is strongly dependent on the dielectric constants of the metal and the dielectric. Here we are interested in the change in the ATR spectra due to dielectric overlayers. Several approximate expressions for the shape of the reflectivity curves in the multilayer geometry (prism-metal-dielectric-vacuum) have been reported.[1,5,7] However, the approximations involved in those derivations are rather significant and we prefer to use an exact formulation. The so-called transfer-matrix method[8] which we outline below is easily amenable to computer calculations.

A wave propagating with a wave vector $k_{||}$ along the interface in the jth medium can be written in the form

$$\mathbf{E}_j^{\pm}(\mathbf{r},t)=\mathbf{E}_j^{\pm}\exp[(\pm\alpha_j z)+i(k_{||}x-\omega t)]\ ,$$

where the z direction is normal to the interface and the x direction is along the interface. The Maxwell equations require $\alpha_j^2=k_{||}^2-\epsilon_j(\omega/c)^2$. The boundary conditions for the interface between medium $j+1$ and j for each component of the electric field lead to the relation:

$$[E_{j+1}]=\mathbf{T}^{j+1,j}[E_j]\ , \tag{1a}$$

where we have written the electric fields in the form of vector:

$$[E_j]=\begin{bmatrix}E_j^+\\E_j^-\end{bmatrix}. \tag{1b}$$

$\mathbf{T}$ is a transfer matrix given by

$$\mathbf{T}^{j+1,j}=\begin{bmatrix}1+Z & 1-Z\\1-Z & 1+Z\end{bmatrix} \tag{2}$$

where $Z=\alpha_j/\alpha_{j+1}$ for TE modes and $Z=\epsilon_j\alpha_{j+1}/\alpha_j\epsilon_{j+1}$ for the x component of TM modes. ϵ_j is the dielectric constant of the jth layer. To account for phase and amplitude changes due to propagation of waves in medium j we introduce a "propagation" matrix $\mathbf{P}^j(d)$:

$$\mathbf{P}^j(d)=\begin{bmatrix}\exp(\alpha_j d) & 0\\0 & \exp(-\alpha_j d)\end{bmatrix}, \tag{3}$$

where d is the layer thickness. The field amplitudes in the prism for Kretschmann geometry can now be written as

$$[E_p]=\mathbf{T}^{pm}\cdot\mathbf{P}^m(d_m)\cdot\mathbf{T}^{mv}[E_v]\equiv\mathbf{M}[E_v] \tag{4}$$

where the indices p, m, and v refer to prism, metal, and vacuum, respectively. The effective transfer matrix $\mathbf{M}$ relates fields in the vacuum to those in the prism. It can now be shown that for incident angles (ϕ_i) greater than the angle of total internal reflection, i.e., for $k_{||}=(\omega/c)(\epsilon_p)^{1/2}\sin(\phi_i)>(\epsilon_v)^{1/2}\omega/c$, the reflectivity is given by

$$R=|m_{11}/m_{12}|^2, \tag{5}$$

while the dispersion relation of SPP is given by $m_{11}=0$ (m_{11} and m_{12} are the elements of matrix $\mathbf{M}$). The solution of the dispersion relation (possible only for TM fields) yields a complex propagation vector. The real $k_{||}$-vector scan [as is the case in the Kretschmann geometry $k_{||}=(\omega/c)(\epsilon_p)^{1/2}\sin(\phi_i)$] will show a reflectivity dip in the vicinity of an SPP resonance.

The presence of a dielectric overlayer on the metal surface will change the metal-vacuum transfer matrix $\mathbf{T}^{mv}$. For an overlayer of macroscopic thickness d_d, the new transfer matrix is obtained by the following substitution in Eq. (4):

$$\mathbf{T}^{mv}=\mathbf{T}^{md}\mathbf{P}^d(d_d)\mathbf{T}^{dv}. \tag{6}$$

For submonolayer and monolayer coverages, the thickness d_d is no longer a macroscopic quantity and the transfer matrix $\mathbf{T}^{mv}$ should in principle be calculated microscopically. A few such calculations have been attempted.[9,10] Dignam and Fedyk[9] showed that ignoring image and retardation effects the optical response of a two-dimensional array of point dipoles is still given by the usual Lorentz-Lorenz expression $(\epsilon-1)/(\epsilon+2)=\frac{4}{3}\alpha\pi N_s/d$, provided that an effective thickness

$$d_0=\tfrac{8}{3}\pi\alpha N_s/\Sigma \tag{7a}$$

is used. Here, α is the molecular polarizability, N_s is the surface number density of molecules for a completely filled monolayer, and Σ is the dipole sum. Assuming a square net (the dipole sum is only weakly dependent on the structure[11]), we have $d=0.935a$ (Ref. 9), where a is the nearest-neighbor distance. Extrapolation to submonolayer coverages is straightforward; $N_s\rightarrow N=\Theta N_s$ and $\Sigma\rightarrow\Sigma(\theta)$ where Θ is the fractional coverage ($\Theta=N/N_s$). According to Mahan and Lucas[11] the average dipole sum for a randomly filled array is $\Sigma(\Theta)=\Theta\Sigma(1)$. Thus for a submonolayer whose saturation coverage is N_s the effective dielectric constant is

$$\epsilon=1+\frac{4\pi\alpha\Theta N_s/d_0}{1-\frac{4}{3}\pi\Theta\alpha N_s/d_0} \tag{7b}$$

with thickness d_0 still given by Eq. (7a).

Inclusion of the image dipole contribution to the local field leads[9] to an effective thickness given by

$$d^{-1}=d_0^{-1}+d_i^{-1} \tag{8a}$$

and the effective dielectric constant

$$\epsilon=1+\frac{4\pi\Theta N_s\alpha(d_0^{-1}+d_i^{-1})}{1-\frac{4}{3}\pi\Theta N_s\alpha d_s^{-1}+4\pi\Theta N_s\alpha d_i^{-1}}, \tag{8b}$$

where $d_i=\frac{8}{3}\pi N_s(X/3)/\Sigma(h)$, and $\Sigma(h)$ is the dipole sum for images

$$\Sigma(h)=\frac{1}{a^3}\left[\sum_{m=n\neq 0}\frac{m^2+n^2-2h^2}{(m^2+n^2+h^2)^{5/2}}-\frac{2}{h^3}\right]. \tag{8c}$$

Here $h=z/a\,(h\neq 0)$, z is the dipole-image distance, and X is the imaging parameter given by $X=(\epsilon_m-1)/(\epsilon_m+1)$.

For highly reflecting metals the imaging parameter X can be approximated by $\mathrm{Re}(X)$, so that both d and ϵ remain real-valued. An advantage of Dignam's formulation is that it provides an explicit expression for the effective thickness of partially filled monolayers. This is an improvement over the more commonly used[12] macroscopic approach, where the molecular dimension of adsorbed molecules is arbitrarily taken for d.

Another macroscopic approximation has been used by Weber[4] in his work on the oxidation of copper. Starting with an approximate expression for the change in the SPP propagation vector due to an overlayer of thickness d_d and the dielectric constant ϵ_d:

$$\frac{\delta k_{||}}{k_{||}}=\frac{\omega^2\epsilon_m\alpha_m\alpha_v}{c^2k_{||}^2(\epsilon_m\alpha_m+\alpha_v)}\frac{(\epsilon_d-1)(\epsilon_m-\epsilon_d)d_d}{(\epsilon_m+1)\epsilon_d} \tag{9}$$

and setting $\epsilon_d-1=4\pi N\chi/d$ in the numerator and $\epsilon_d=1$ otherwise, one obtains

$$\frac{\delta k_{||}}{k_{||}}=\frac{\omega^2}{c^2k_{||}^2}\frac{\epsilon_m\alpha_m\alpha_v(\epsilon_m-1)}{(\epsilon_m\alpha_m+\alpha_v)(\epsilon_m+1)}4\pi N\chi, \tag{10}$$

where χ is the molecular susceptibility of the adsorbed species. Although this model is expected to be valid only in the extremely dilute regime ($\Theta\ll 1$), because of neglect of the Lorentz-Lorenz corrections, it demonstrates important features of the SPP response to dielectric overlayers. The wave-vector shift $\delta k_{||}$ is approximately linear in the product of coverage and polarizability, and for typical metals and nonlossy overlayers the relative change in the

imaginary part $\mathrm{Im}(\delta k_{||})$ is much smaller than that in $\mathrm{Re}(\delta k_{||})$.

Figure 1 shows the calculated ATR response, i.e., shift in the resonance dip position as a function of coverage. The image dipole sum [Eq. (8c)] was estimated numerically. The polarizability is that of pyridine in the gas phase. The calculations are for Weber's model (dashed curve) and for Dignam's model (solid curves). The latter is calculated for several values of parameter h. The $h=\infty$ case corresponds to a situation where the image effects are neglected. As expected, inclusion of image dipoles increases the shift of the resonance dip position. The magnitude of this effect is strongly dependent on the position of the image plane, For $h>1$ which corresponds to image plane separation greater than the nearest-neighbor distance, the effect is essentially negligible. In the small coverage limit Weber's approximation converges to that of Dignam's, as expected. Before concluding this section we note that the dielectric constant as given by Eq. (7b) will diverge when $\alpha\Theta N_s/d$ approaches $\frac{3}{4}\pi$. This has an important consequence in fitting experimental data, as small changes in the polarizability and the monolayer coverage near the divergence point will result in large effects on the position of the ATR dip.

III. EXPERIMENTAL

In order to avoid contamination of silver films, all experiments reported here were carried out in an UHV chamber (base pressure of about 2×10^{-10} Torr) equipped with evaporation and dosing systems. The experimental arrangement is shown schematically in Fig. 2. A hemicylindrical prism P (BK-7 glass, $\epsilon_p\simeq2.31$) is mounted on a modified UHV manipulator M with cooling and heating capabilities (105—550 K). The silver film was grown on the flat side of the prism by evaporation of Ag pellets of 99.995% purity from a shielded tantalum boat EB. The evaporation rate was monitored by a quartz thickness gauge TM. Evaporation rates were 2—20 Å/s and the final thickness was approximately 500 Å. The pressure rise during evaporation never exceeded 3×10^{-8} Torr. After evaporation the prism was rotated toward an optical window W. The monochromatic p-polarized beam from either an argon-ion or a helium-neon laser enters the prism after reflection from two mirrors M_1 and M_2. Its collimation inside the prism is assured by the focusing lens L_4. Normal incidence (i.e., no refraction of the beam when it enters the prism) could be easily established by observing the reflection from the curved side of the prism. The angle of incidence ϕ_0 is then given by

$$2\phi_0=2\alpha_1+2(180^\circ-\alpha_2)+\alpha_3 \tag{11}$$

where $\alpha_1,\alpha_2,\alpha_3$ are the angles mirrors M_1,M_2 and the exit beam make with the incident beam (here horizontal). Mirror M_1 is mounted on a high-precision rotation stage. The vacuum mirror M_2 uses a low-resolution rotary feedthrough—its calibration is easily accomplished by retroreflection. The ATR spectra (i.e., reflectivity versus k,ω) were measured in the so-called angular scan where the incident light frequency is kept constant while the interface wave vector $k_{||}$ is scanned by changing the incident angle.

Scanning is accomplished by translation of the outside mirror M_1 in the direction of the incident beam. Refraction at the curved surface of the prism deviates the beam inside the prism by the amount

$$\Delta\phi=(\phi_i-\phi_0)$$
$$=\arcsin(d/R)-\arcsin(d/R\sqrt{\epsilon})\ , \tag{12}$$

where ϕ_i is the incident angle, $d=(x-x_0)\sin(2\alpha_1)$, x is the mirror position, R is the prism radius, ϵ is the dielectric constant of the prism, and the zero subscripts denote

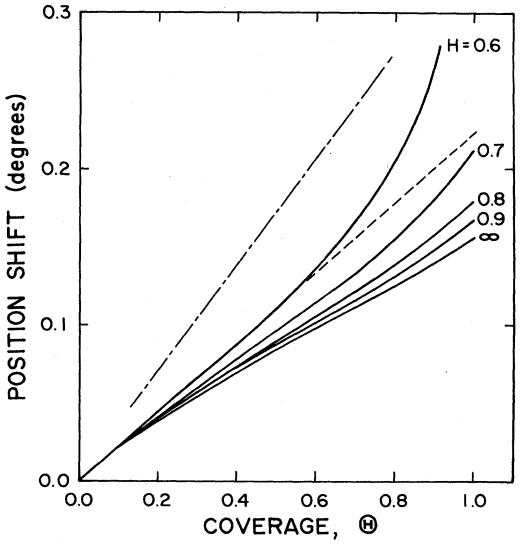

FIG. 1. Shift in position of the ATR dip as a function of pyridine coverage calculated for the Weber approach (dashed line) and Dignam's model (solid lines). Labels indicate the position of the image plane ($h=z/a$). Experimental data, dashed-dotted line. Calculations are for $\lambda=4579$ Å, $\epsilon_p=2.32$, $\epsilon_{AG}=-7.44+i0.284$, $d_{Ag}=500$ Å, $\alpha=9.7\times10^{-24}$ cm^3, $N_s=5\times10^{14}$ cm^{-2}.

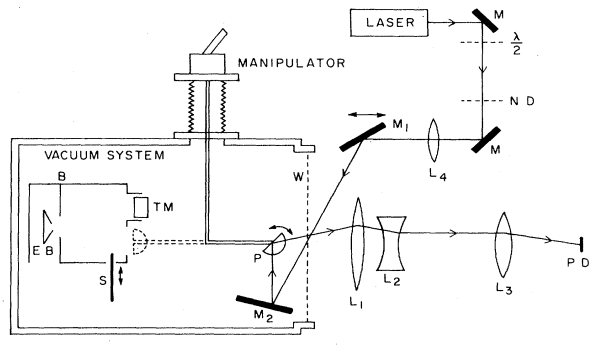

FIG. 2. Light path and evaporation apparatus for this experiment. $\lambda/2$, half-wave plate; ND, neutral density filter; L_4, laser focusing lens; M_1, motor driven mirror; W, window; M_2, externally adjustable mirror in UHV system, P, prism; L_1, L_2, and L_3 form an optical relay; PD, photodiode of power meter. B, TM, S, and EB are a stainless steel box, a thickness monitor sensor, a shutter, and an evaporation boat.

normal incidence. In our experiment the sensitivity $\Delta\phi/(x-x_0)$ is typically $\simeq 3$ deg/mm which is sufficiently high to detect the SPP resonance shifts due to a fraction of a monolayer of pyridine. Movement of the beam across the metal film as the incident angle is scanned and the collection optics aperture limit the useful scanning range to approximately 12°. Lenses $L1$, $L2$, and $L3$ refocus the reflected beam onto a stationary photodetector PD. Transmission of the optical system can be determined from the reflectivity of the s-polarized light or the reflectivity of the p-polarized light from the uncoated part of the prism. The advantages of this method of scanning are (i) only minor modifications to the UHV chamber are required and (ii) the mechanical motions are linear and involve only one moving part (mirror M_1). Scan nonlinearity (in ϕ) and the beam walk are also present in other methods which use triangular prisms.

Since the optical properties of Ag films are known to change after evaporation,[13] we allowed for an overnight anneal (300 K) in the UHV chamber. Before exposure the prism is cooled to 110 K by liquid nitrogen. We used spectroscopic grate pyridine and deionized (18 MΩ cm) water. Both liquids were frozen at −76° C and pumped on before being used in order to remove dissolved gases. The exposures were monitored with a mass spectrometer. No correction for ion-gauge sensitivity to pyridine was applied, and we report exposures in uncorrected langmuirs (1 langmuir = 1 L = 10^{-6} Torr s).

The ATR spectra were originally recorded on the chart recorder and were subsequently digitized for computer processing. This included corrections for reflectivity losses at the prism surface as well as the conversion of the mirror position into the incidence angle according to Eq. (12). The example of the ATR spectra taken after the silver film was exposed to various quantities of pyridine is shown in Fig. 3.

IV. RESULTS AND DISCUSSION

The SPP response to pyridine overlayers, i.e., change in the position and in the width of the resonance dip as a function of exposure, is shown in Fig. 4. The actual exposures are higher than indicated ($\sim 50\%$ at 4 L as estimated below) due to the finite pumping speed. However, the wavelength dependence is correct—the 4579- and 6328-Å ATR spectra were taken simultaneously with colinear laser beams. The data taken at other wavelengths (5145 and 4800 Å) were qualitatively similar to those taken at 6328 Å. It is apparent from Figs. 4(a) and 4(b) (see also the actual ATR traces in Fig. 3) that in addition to the wave-vector shift, the presence of the pyridine overlayer significantly dampens the SPP resonance. Within the framework of the theoretical models presented in Sec. II, such effect is expected to arise from lossy or resonant overlayers. We will see, however, that there is a good reason to believe that this is not the case here. Figure 4 also shows that there is a qualitative difference between lower (<4 L) and higher exposure responses. This is especially evident in the 4579-Å data where the initially positive shift (i.e., toward larger wave vectors) is reversed for exposures between 4 and 18 L. Also the broadening of the ATR dip which is negligibly small for the first data point becomes much more pronounced at higher coverages. The exposure at which those changes in response are observed corresponds roughly to that where discontinuous changes in the ultraviolet photoemission spectros-

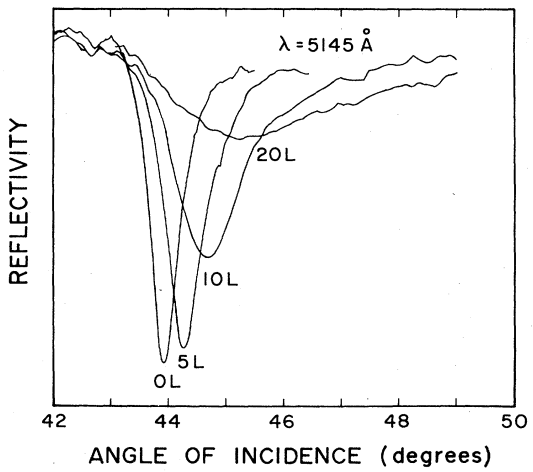

FIG. 3. ATR spectra of silver film covered with various quantities of pyridine.

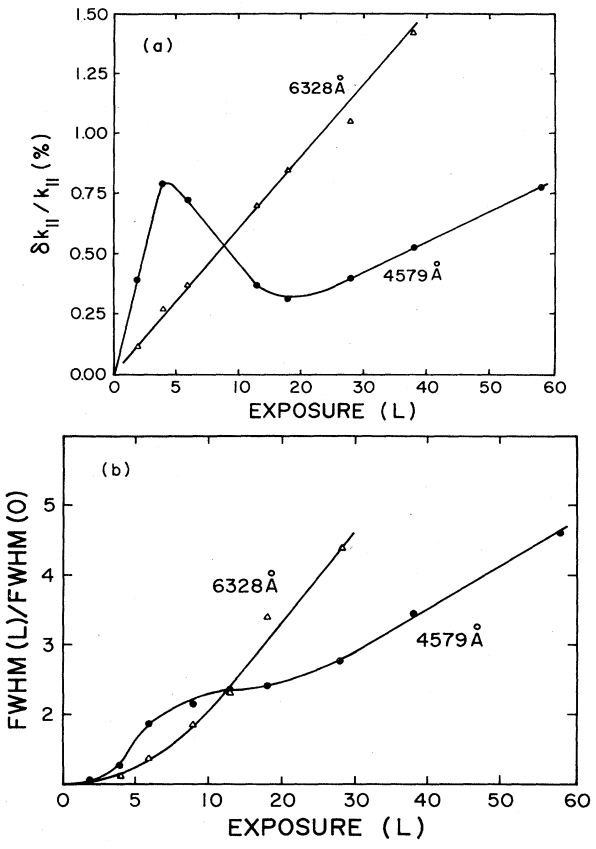

FIG. 4. SPP response to various pyridine exposures; (a) relative change in the resonance wave vector $k_{||}$, (b) full width at half minimum (FWHM) normalized to that of unexposed silver film. Solid lines are guides to the eye only.

copy (UPS) and Auger data are seen.[14–16] Since those are usually interpreted as due to completion of the first monolayer,[14–16] we shall refer to the (0—4)-L exposure range as the submonolayer regime.

A. Submonolayer regime

The submonolayer data (Fig. 5) were taken by continuously monitoring the position of the resonance dip during the exposure. This method of taking data has the advantage over that used for Figs. 3 and 4 in that it avoids ambiguities in exposure associated with the finite pumping speed. Using the exposure at which the first monolayer is formed (6 and 4 L for Fig. 5 and Fig. 4, respectively) we see that the exposures in Fig. 4 are underestimated by approximately 50% at 4 L. Below 6 L, that is for submonolayer coverages, the shift in the ATR dip position is essentially linear over much of the exposure range. Similar linearity of the position shift versus exposure is observed at two other wavelengths studied (6328 and 4880 Å). The magnitude of the shift in the dip position is 0.87, 0.40, and 0.33 mrad/L for 4579, 4880, and 5145 Å, respectively. The 4579-Å data are also sketched in Fig. 1 for comparison with model calculations. The polarizability used in the calculations (9.7 $Å^{-3}$) is that of pyridine in the gas phase. Figure 1 shows that the experimental data cannot be accounted for by either of the models if the pyridine polarizability has the same value as in the gas phase and if the saturation coverage is $N_s = 5\times10^{14}$ cm^{-2}. The linearity of the shift in the ATR dip position versus coverage is in agreement with Weber's approximation, if we assume a coverage-independent sticking coefficient. Equation (10) then yields the product of polarizability and coverage. If we use the estimated saturation coverage 5×10^{14} cm^{-2} (Ref. 14) the pyridine polarizability is 9 $Å^3$ at 4880 and 5145 Å, and 14 $Å^3$ at 4579 Å. For comparison the gas-phase polarizabilities are[17] 11 $Å^3$ and 12 $Å^3$ along the two directions in the plane of a ring and 6 $Å^3$ normal to the ring.

Weber's approximation ignores the local-field effects.

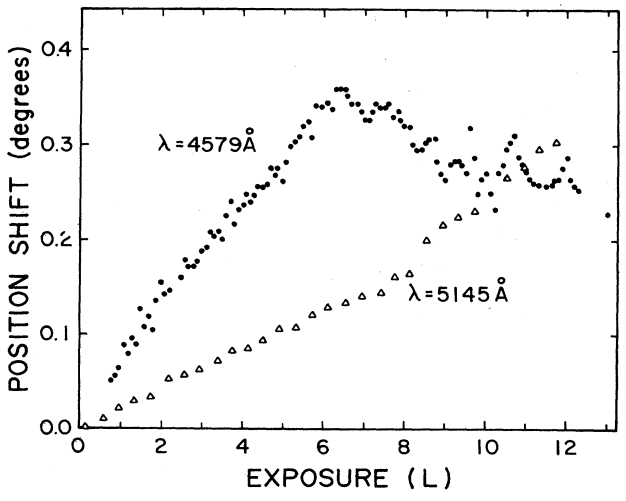

FIG. 5. Shift in position of the ATR reflectivity dip as a function of pyridine exposure.

However, Dignmam's model, which includes those explicitly, does not predict a linear response. This is not necessarily inconsistent with experimental results, as the coverage dependence of the sticking coefficient and of the average orientation of adsorbed molecules are not known. We avoid this complication by calculating the response for a completely filled monolayer, i.e., at the exposure at which the slope of the dip position shift versus exposure curve changes discontinuously. If we ignore image effects and assume again $N_s = 5\times10^{14}$ cm^{-2}, the pyridine polarizability is $\sim$14.5 $Å^3$ at all three wavelengths. Thus, if the upper limit on the saturation coverage is 5×10^{14} cm^{-2} as indicated by the UPS work[14] the effective polarizability is enhanced. By effective polarizability we mean the polarizability which accounts for both image effects and chemisorption induced changes in the silver substrate and in the adsorbed molecule. It would be interesting to try to separate out the image effects. That, however, requires knowledge of the image plane position. Since estimations for the pyridine-silver system vary significantly,[18] we do not feel that explicit inclusion of the image effects is justified at this stage. The chemisorption effects, which also may contribute to the observed enhancement of the effective polarizability of the pyridine-silver system, should be dependent on bonding between the molecule and metal surface. The silver films used in our experiments are polycrystalline, and the bonding for pyridine on such surfaces may be different from that on a single-crystal surface or on a SERS-active surface (cold film). The fact that the image effects should be adsorbate independent as opposed to chemisorption-induced changes, provides an experimental opportunity to distinguish between these two cases.

We will report soon on the experiments involving other molecules as well as a more detailed study of the wavelength dependence.

B. High-exposure regime (> 6 L)

The data of Fig. 5 show a discontinuous change in the SPP response at approximately 6-L exposure for both wavelengths. This exposure corresponds to the saturation coverage for the first monolayer.[14–16] Therefore, it is tempting to ascribe the break in the response to a difference in the sticking coefficient between the first and the second monolayer. This, however, cannot account for a drastic and wavelength-dependent broadening of the SPP resonance [see Fig. 4(b)] as well as the negative (i.e., toward lower values) shift in $k_{||}$ observed for 4579 Å. One could postulate that the observed changes are due to the different optical properties of the subsequent monolayer from those of the first monolayer. Then the ATR response should be given by some combination of the effective dielectric constant and the thickness. We therefore attempted to fit the multilayer spectra to the theoretical reflectivity curves [as given by Eqs. (4)—(6)] using a least-squares procedure. However, no physically meaningful complex dielectric constant and thickness could be obtained, indicating that in this exposure regime the ATR response is dominated by other effects. The theoretical model presented in Sec. II assumes uniform layers and

sharp boundaries. In reality the interface is always rough to some extent. The SPP propagating on such an interface will have its lifetime reduced due to roughness induced scattering. The additional scattering channels include scattering into bulk plasmons, other SPP's and into volume electromagnetic modes. For Ag films evaporated at room temperature the effect of interface scattering is small.[13] The fact that we could fit our unexposed film data with the published dielectric constant[13] shows that our films are as smooth as those reported in the literature. However, for the silver film covered by a disordered overlayer the roughness scattering may not be negligible.

To test this hypothesis we measured the intensity of the diffusely scattered light as a function of exposure to pyridine. In this experiment the 4579-Å light was incident at $\sim 35°$ from the interface normal on the flat side of the prism and the light intensity scattered along the normal to the interface was measured. The results are shown in Fig. 6. No detectable changes are observed below 6 L. Further exposure results in a steplike increase in the scattering intensity at ~ 6 L and a continuous increase afterwards. Figure 6 also shows similar data for water. No increase in the scattering intensity is observed in this case. The ATR spectra of water show no additional broadening of the reflectivity dip and can be fitted with the theoretical model in which the water overlayer is represented by a layer of uniform thickness d. Excellent fits were obtained with the published value of the dielectric constant of ice [1.74 (Ref. 19)] for coverages up to 180 L (~ 340 Å).

The combined ATR and diffuse reflectivity data for pyridine and water thus led us to believe that the ATR response to pyridine at high coverages (> 6 L) is dominated by overlayer roughness effects. We conclude that the pyridine overlayer undergoes a structural transformation upon completion of the first monolayer, resulting in a rough surface. Increase in the diffuse scattering strength with further exposure strongly suggests that the pyridine does not condense in a layer-by-layer fashion.

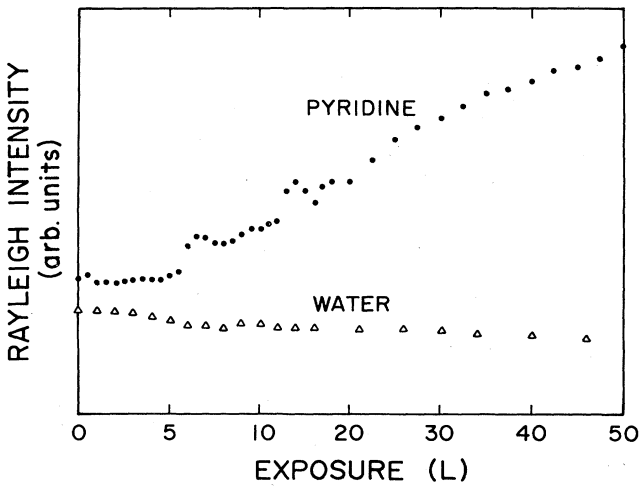

FIG. 6. Intensity of diffusely scattered light as a function of pyridine exposure. Experimental conditions are $\lambda = 4579$ Å, $\phi_i = 35°$, $\phi_{\text{scatt}} = 0° \pm 5°$, $T_{AG} = 105$ K.

Our conclusion that the ATR response above 6 L is dominated by roughness scattering is further corroborated by two other experiments. We did a "spacer experiment" in which the pyridine was condensed on an overlayer of water adsorbed directly on the metal surface. The thickness of the water spacer was ~ 80 Å as determined by the least-squares fit to the ATR spectrum. No significant broadening of the ATR dip was observed for up to ~ 40 L of pyridine exposure, above which strong scattering took place. This indicates that the condensation process depends on the nature of the substrate. Also in the preliminary ATR study of pyridine liquid,[20] the SPP resonance is still found (at 5145 Å), with only slightly broadened width.

Under suitable conditions, the SPP resonance can lead to a strong enhancement of electromagnetic fields at the metal interface.[21] From the data presented here it is rather clear that the magnitude of the field enhancement will be strongly dependent on pyridine coverage. Such an effect has been seen in the experimental data of Sanda *et al.*[16] They used the SPP resonance excited on the silver grating to enhance the Raman signal from pyridine overlayers. Their Raman data show a strong decrease in the enhancement factor between the first and the second layer. The effect discussed above may be responsible for at least part of their observed coverage dependence.

V. CONCLUSIONS

To conclude, we have measured the changes in the surface-plasmon resonance of the silver film as a function of pyridine coverage. The submonolayer response is linear, i.e., the interface wave vector $k_{||}$ at which the resonance is observed shifts linearly with exposure. No significant broadening of the reflectivity dip is observed in this coverage regime, indicating that the pyridine overlayer is not lossy. Using the estimated saturation coverage, we calculate the effective polarizability that is enhanced (~ 14.5 Å^3 versus ~ 9.7 Å^3 for the gas phase). Such an enhancement may be due to image effects or chemisorption effects. For coverages above the first monolayer the SPP resonance of the silver film is strongly damped. Diffuse reflectivity data as well as other experimental evidence strongly suggest clustering of the pyridine molecules in this coverage regime.

Our results have several implications for SERS. Firstly, the modification of the pyridine polarizability due to chemisorption effects is rather small. Thus it is rather unlikely that the pyridine-metal system has an excitation level which couples strongly with light in the visible range.

Finally, in the situation where the SPP resonance is the major enhancement mechanism, the enhancement factor will be much smaller for exposures > 6 L than that for exposures < 6 L due to the strong damping of the SPP resonance.

ACKNOWLEDGMENT

This work was supported by the Department of Energy under Grant No. DE-AT03-81ER10820.

[1]*Surface Enhanced Raman Scattering,* edited by R. K. Furtak and T. E. Furtak (Plenum, New York, 1982).
[2]J. E. Demuth and P. N. Sanda, Phys. Rev. Lett. **47**, 57 (1981).
[3]A. Tadjeddine and D. M. Kolb, J. Electroanal. Chem. **111**, 119 (1980).
[4]W. H. Weber, Phys. Rev. Lett. **39**, 153 (1977).
[5]W. P. Chen and J. M. Chen, Surf. Sci. **91**, 601 (1980).
[6]K. Bhasin, D. Brayan, R. W. Alexander, and R. J. Bell, J. Chem. Phys. **64**, 5019 (1976).
[7]E. Kretschmann and H. Raether, Z. Naturforsch. **A23**, 2135 (1968).
[8]F. Abeles, Ann. Phys. (Paris) **5**, 598 (1950).
[9]M. Dignam and J. Fedyk, J. Phys. (Paris) Colloq. **38**, C5-57 (1977).
[10]D. V. Sivukhin, Zh. Eksp. Teor. Fiz. **21**, 367 (1951).
[11]G. D. Mahan and A. A. Lucas, J. Chem. Phys. **68**, 1344 (1978).
[12]F. H. P. M. Habraken, O. L. J. Gilzeman, and G. A. Bootsma, Surf. Sci. **96**, 481 (1980).
[13]W. H. Weber and S. L. McCarthy, Phys. Rev. B **12**, 5643 (1975).
[14]J. E. Demuth, K. Christmann, and P. N. Sanda, Chem. Phys. Lett. **76**, 201 (1980).
[15]M. Udagawa, Chih-Cong Chou, J. C. Hemminger, and S. Ushioda, Phys. Rev. B **23**, 6843 (1981).
[16]P. N. Sanda, J. E. Demuth, J. C. Tsang, and J. M. Warlaumont, in *Surface Enhanced Raman Scattering,* Ref. 1, p. 189.
[17]A. K. Burnham and T. D. Gierke, J. Chem. Phys. **73**, 4822 (1980).
[18]G. C. Schatz, in *Surface Enhanced Raman Scattering,* Ref. 1, p. 34.
[19]A. Ehringhaus, Neues Yahrb. Mineral. Geol. Beilage Band B **41**, 342 (1917).
[20]K. Kurosawa (private communication).
[21]S. Ushioda and Y. Sasaki, Phys. Rev. B **27**, 1401 (1983).